Journal of Applied Electrochemistry (2024) 54:341–360
https://doi.org/10.1007/s10800-023-01956-2

RESEARCH ARTICLE

An investigation of energy utilization behavior on borosilicate glass through heating and stirring of the electrolyte in electro-chemical discharge machining

Dil Bahar[1] · Akshay Dvivedi[1] · Pradeep Kumar[1]

Received: 6 April 2023 / Accepted: 22 July 2023 / Published online: 7 August 2023

Abstract
Owing to its non-conducting nature, Through Glass Vias (TGV) is a new paradigm to reduce the losses in high-frequency transmission systems. However, due to brittleness and non-conducting nature, micro-machining of glass is challenging. In the backdrop of limitations of the existing processes, Electro-chemical Discharge Machining (ECDM) is an evolutionary micro-machining process for brittle and non-conducting materials, like glass. ECDM is a hybrid of electro-chemical and electro-discharge processes. During machining in ECDM, poor flushing coupled with poor replenishment of electrolyte deteriorates the Energy Utilization Behavior (EUB), particularly in hydrodynamic regime. Therefore, the present article deals with a novel approach (using a magnetic stirrer) of Temperature-assisted ECDM (termed as T-ECDM) to improve the energy utilization behavior in the micro-machining of borosilicate glass. The T-ECDM approach has the capability to control the temperature and stirring rate of the electrolyte. The Machining Rate (MR) as well as Aspect Ratio (AR) of micro-hole are considered as the desirable performance indicator, while Tool Wear Ratio (TWR) and Heat-Affected Zone (HAZ) are considered undesirable performance indicator of EUB. The experimental investigation indicated the improvement in Overall Energy Utilization Index (OEUI) by T-ECDM as compared to ECDM. The morphological, composition analysis, and surface profiles of micro-hole witnessed the improved flushing and etching in T-ECDM than ECDM that resulted in better surface finish of the micro-hole. It implies better energy utilization behavior in terms of surface characteristics also.

✉ Pradeep Kumar
pradeep.kumar@me.iitr.ac.in

Dil Bahar
dilbahar@me.iitr.ac.in

Akshay Dvivedi
akshaydvivedi@me.iitr.ac.in

[1] Advanced Manufacturing Processes Laboratory, Department of Mechanical and Industrial Engineering, Indian Institute of Technology (IIT) Roorkee, Roorkee 247667, India

Graphical abstract

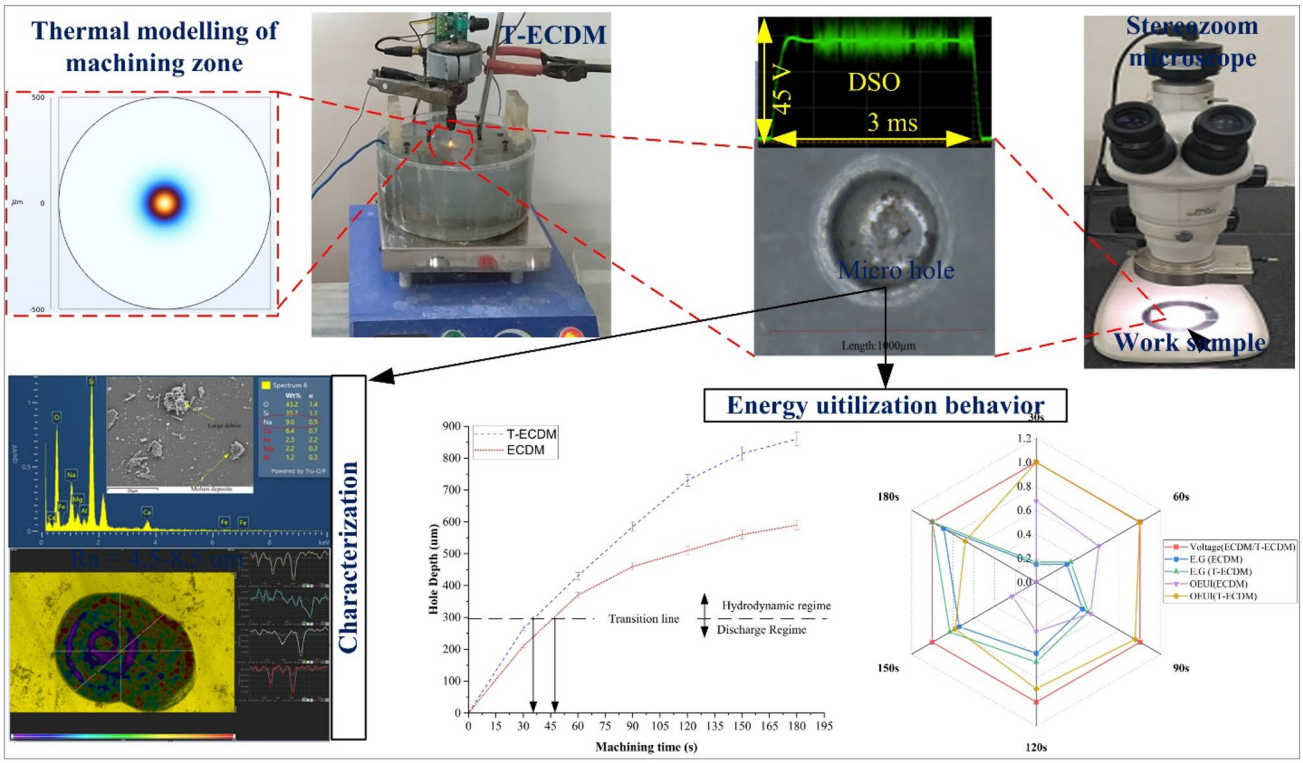

Keywords Silicon · TGV/TSV · Energy · Magnetic · Characterization · Micro-machining

List of symbols

ECDM	Electro-chemical discharge machining
T-ECDM	Temperature-assisted ECDM
TGV	Through glass vias
TSV	Through silicon vias
MEMS	Micro-electro-mechanical system
EUB	Energy utilization behavior
MR	Machining rate
AR	Aspect ratio
TWR	Tool wear rate
HAZ	Heat-affected zone
OEUI	Overall energy utilization Index
LBM	Laser beam machining
USM	Ultra sonic machining
AJM	Abrasive jet machining
DC	Direct current
ECC	Electro-chemical cell
FESEM	Field emission scanning electron microscope
EDS	Energy-dispersive spectroscopy
ρ_b	Gas bubble density
ρ_l	Electrolyte density
γ	Contact angle (mean) between electrode and bubble.
R	Bubble radius
V_b	Bubble volume
σ	Surface tension at the interface of bubble with electrolyte
∅	Receding angle
θ	Advancing angle
R_s	Spark radius
T_e	Electrolyte temperature
P_e	Partition energy
k	Electrical conductivity
K	Thermal conductivity
α	Temperature coefficient
ρ	Density of the workpiece
C_p	Specific heat (at constant pressure)
EG	Energy generated

1 Introduction

Scalability is the major challenge for on-chip interconnects, for which Through Silicon Vias (TSV) is a promising solution [1]. However, due to semiconductor nature of silicon, TSV results in huge losses in high-frequency transmission

systems [2]. Therefore, due to non-conducting nature, transparency, and chemical inertness, TGV is a new paradigm for radio frequency-based Micro-ElectroMechanical Systems (MEMS) to reduce the losses in the 5G wireless transmission systems [3]. TGV is prepared by micro-machining the holes in the glass substrate, which is challenging due to brittleness and non-conducting nature of the glass. In the current scenario to realize the industrial objective, intellectuals and researchers are trying non-conventional micro-machining processes. In non-conventional processes, Laser Beam Machining (LBM) requires expensive equipment and uses thermal energy that creates micro-cracks that limit the industrial applicability. Mechanical energy-based processes such as Ultrasonic Machining (USM) and Abrasive Jet Machining (AJM) are capable of micro-machining the hard and brittle materials irrespective of their conductive nature [4], but results into poor AR of micro-hole. Although chemical-based machining processes produce detailed micro-profiles with good surface finish on several materials, low-dimensional accuracy, low AR, and poor MR are the demerits of chemical-based process. Kura Fuji and Suda proposed the idea of ECDM in 1968 as a novel hybrid production technique that encompasses the characteristics of ECM and EDM to get over these limitations [5]. ECDM process has meticulously machined several advanced materials like (i) glass, (ii) composites [6], (iv) ceramics [7], (vi) E-glass–fiber–epoxy composite material [8], (vii) silicon wafer [9], and (viii) Zirconium oxide [10]. In the past few decades, ECDM has emerged into a favorable option for the u-machining of glass [11]. ECDM is an evolutionary process that is being used on brittle and hard materials for the applications in MEMS and Micro-fluidic devices [12]. Arab et al. [13] experimentally demonstrated the fabrication of TGV using ECDM process. ECDM has been attempted for the fabrication of micro-products from electrically non-conductive materials [14]. Low initial investment and compact size are some of the favorable features of this technology that make it attractive toward micro-fabrication industry. The schematic of ECDM along with tool–energy interaction is demonstrated in Fig. 1; the negative and positive ends of the DC power source are connected, respectively, to the tool and the auxiliary electrode. The state of electrolyte level, work piece, and auxiliary electrode is shown in Fig. 1a.

In ECDM, the hydrogen and Oxygen bubbles are produced at the cathode and anode, respectively, in an electrochemical cell (ECC). The hydrogen gas bubbles come into physical touch with one another and then turns into a gas film, surrounding the tool [15]. This hydrogen gas film formation takes place through electrochemical process [16] and also through Joule heating [17, 18]. The process mechanism of ECDM mainly depends on gas film building mechanism. In electrolysis, the gas film generation rate accelerates with electrolyte conductivity [19], which rises with electrolyte temperature. Interestingly, it is reported that in ECDM, gas film contains extra elements than just hydrogen [16], particularly when NaOH or KOH is used as the electrolyte, ions of potassium or sodium are observed that can be a crucial factor for the behavior of thermal discharges. The hydrogen gas film creates insulation in the proximity of tool electrode that generates an intensive electric field (10^7 V/m) across the film [20] and electrical breakdown of this film causes thermal discharges by bombarding a huge number of electrons, resulting into material removal of work material by melting [21]. At the same time, due to elevated temperature, the chemical etching gets accelerated and causes material removal [22]. In u-ECDM, the material removal and quality characteristics of machined micro-hole are influenced by numerous parameters as shown in Fig. 2. Using these parameters, literature witnessed the use of numerous algorithms and techniques for the parametric optimization of ECDM process [23–25] and energy channelization behavior of the ECDM process [12].

According to Kulkarni et al. [21], 2%–6% of total energy generated (from thermal discharges) in ECDM goes to

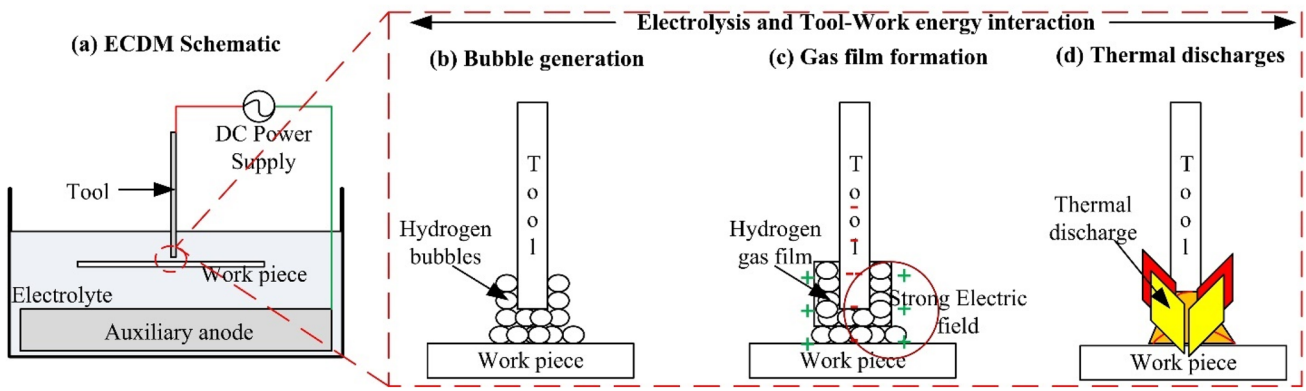

Fig. 1 Schematic diagram of ECDM with tool–work energy interactions

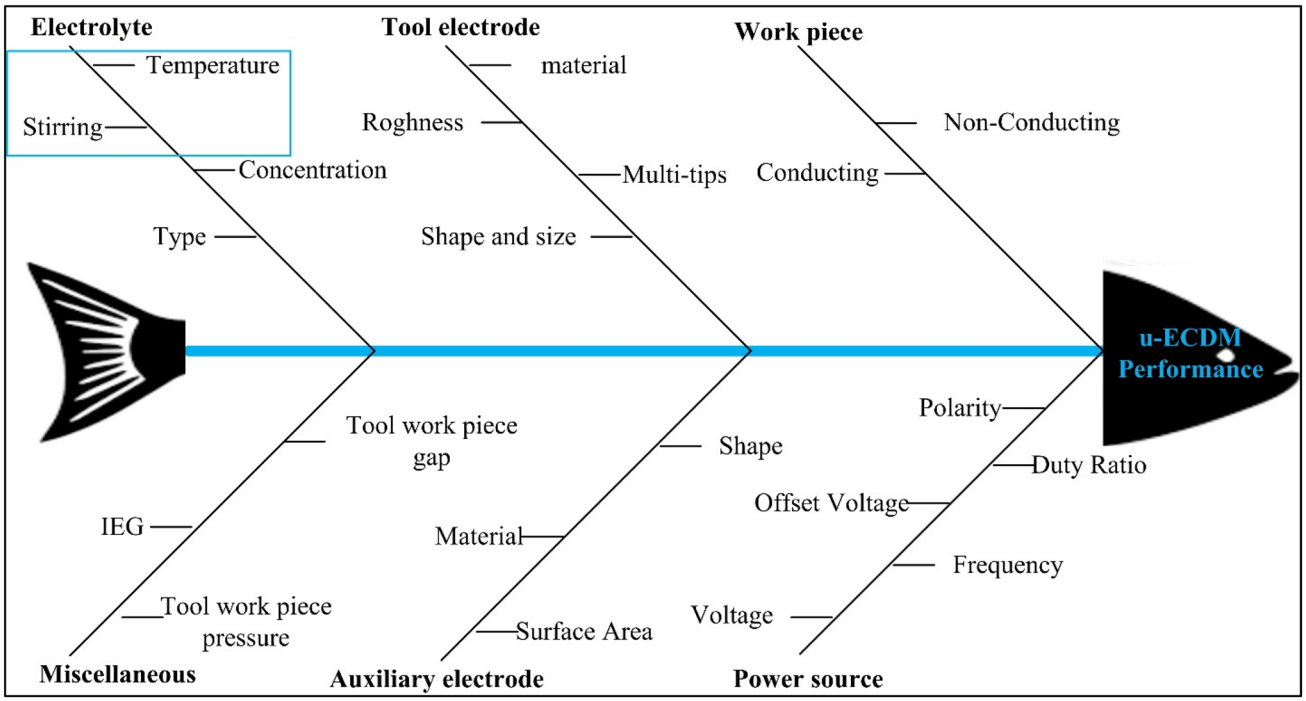

Fig. 2 Fish bone (Ishikawa) diagram for the performance of ECDM

workpiece and 77%–96% energy goes to the electrolyte. In ECDM, micro-machining of hole up to 200–300 um is considered under discharge regime and more than 300 um is considered under hydrodynamic regime [26, 27]. According to published research [28, 29], in the micro-machining of holes, the EUB deteriorates as the hydrodynamic regime approaches owing to accumulation of hydrogen bubbles, sludge/debris formation, and poor electrolyte replenishment in the processing zone. Consequently, the portion of thermal energy utilized toward work piece, electrolyte, and work piece also varies with the change of regime, implying the variation in the performance characteristics too. In literature [12, 30–32], the desirable characteristics (AR and MR) and undesirable characteristics (TWR and HAZ) have been used to correlate the usage of discharge energy in ECDM process; however, a collective investigation (including multiple characteristics) during discharge and hydrodynamic regime is missing from the literature. Singh et al. [30] analyzed the energy channelization behavior of u-ECDM by incorporating Magneto Hydro Dynamics (MHD) on Y-SZ ceramics. Their study concluded 120% rise in the AR of micro-hole owing to MHD. To resolve the problems of ECDM, numerous hybridization techniques are reported in the literature [20]. However, it was observed that ECDM process does not maintain stability throughout machining due to variation in electrolyte temperature during machining and concentration gradient in the electrolyte bath. By virtue of this temperature gradient and concentration gradient, ECDM process exhibits variation in the performance characteristics [33]. Consequently, in literature, ECDM process has been leveled as a stochastic process [34]. Therefore, an approach is required in the ECDM to improve the EUB while maintaining stable machining conditions. Based on literature [35, 36] and author's knowledge, heating and stirring of the electrolyte are expected to fulfill these requirements. The electrolyte temperature and electrolyte stirring are the vital parameters toward the productivity and quality features of machined geometry in ECDM [35, 36]. However, literature reveals that in-depth research is required further in the domain electrolyte temperature and electrolyte stirring. Elevated electrolyte temperature boosts ECDM production and geometric correctness [35], while stirring action in the electrolyte improves the surface finish by restricting the formation of recast layer [36].

1.1 Problem formulation and objectives

As discussed above, the total energy generated by the thermal discharges in ECDM goes to the electrolyte, work piece, and the tool electrode. However, the literature and experimental observations suggest that the portion of energy utilized in the micro-machining of hole (in the workpiece) deteriorates when regime changes from discharge to hydrodynamic. The attributed reasons are accumulation of hydrogen bubbles in the proximity of tool electrode, sludge formation, and poor electrolyte replenishment in the processing

zone [28, 29]. To tackle these problems, the present communication has suggested to incorporate an innovative approach (use of magnetic stirrer) in ECDM (termed as T-ECDM), having the capability to heat and stir the electrolyte. Subsequently, a comparative experimental investigation of T-ECDM with basic-ECDM has been carried out on EUB in discharge as well as hydrodynamic regime. In the present study, EUB has been quantified in terms of desirable characteristics (MR and AR) and undesirable characteristics (TWR and HAZ). The morphology, composition, and surface roughness of micro-holes have been presented to substantiate the EUB. Finally, Overall Energy Utilization Index (OEUI) has been depicted with the help of a radar graph.

2 Materials and methods

In this communication, the setup of T-ECDM facility (Fig. 3) was designed in the laboratory of Advanced Manufacturing Processes (AMP), IIT Roorkee. This setup includes a DC pulsed power source, magnetic stirrer with hot plate, temperature controller and thermocouple, micro tool electrode, auxiliary electrode (Anode), pressurized feeding system (work fixture), and crystallizing dish (made of borosilicate glass). The Digital temperature controller (i-therm, AI-7482) along with a thermocouple controls the electrolyte temperature. Additionally, the stirring action in electrolyte helped in transferring the electrolyte heat (due to thermal discharges) to the ambience by virtue of convection. Consequently, a stable electrolyte temperature was maintained. The auxiliary electrode and tool electrode were connected to the power source's positive terminal and negative terminal, respectively. The discharge behavior during machining was recorded in a Digital Storage Oscilloscope (DSO). In the domain of micro-machining, the use of magnetic stirrer with ECDM is a novel approach in the present study. The function of magnetic stirrer (with hot plate) is to control the electrolyte temperature and stir the electrolyte. In magnetic stirrer, the function of hot plate is to heat up the electrolyte and rotating magnetic bead (by virtue of rotating magnetic field) stirs the electrolyte. Due to good performance in ECDM, aqueous NaOH was preferred as the electrolyte [32]. Borosilicate glass has been chosen as the workpiece owing to its tremendous applications at micro-level. The chemical and mechanical properties of borosilicate glass were considered from the literature [37]. A dedicated pressurized work feeding system has been used to hold and feed the workpiece. The rationale of using the pressurized feeding system is to keep the minimal consistent working gap (nearly nil) throughout the machining process, which lowers performance variance.

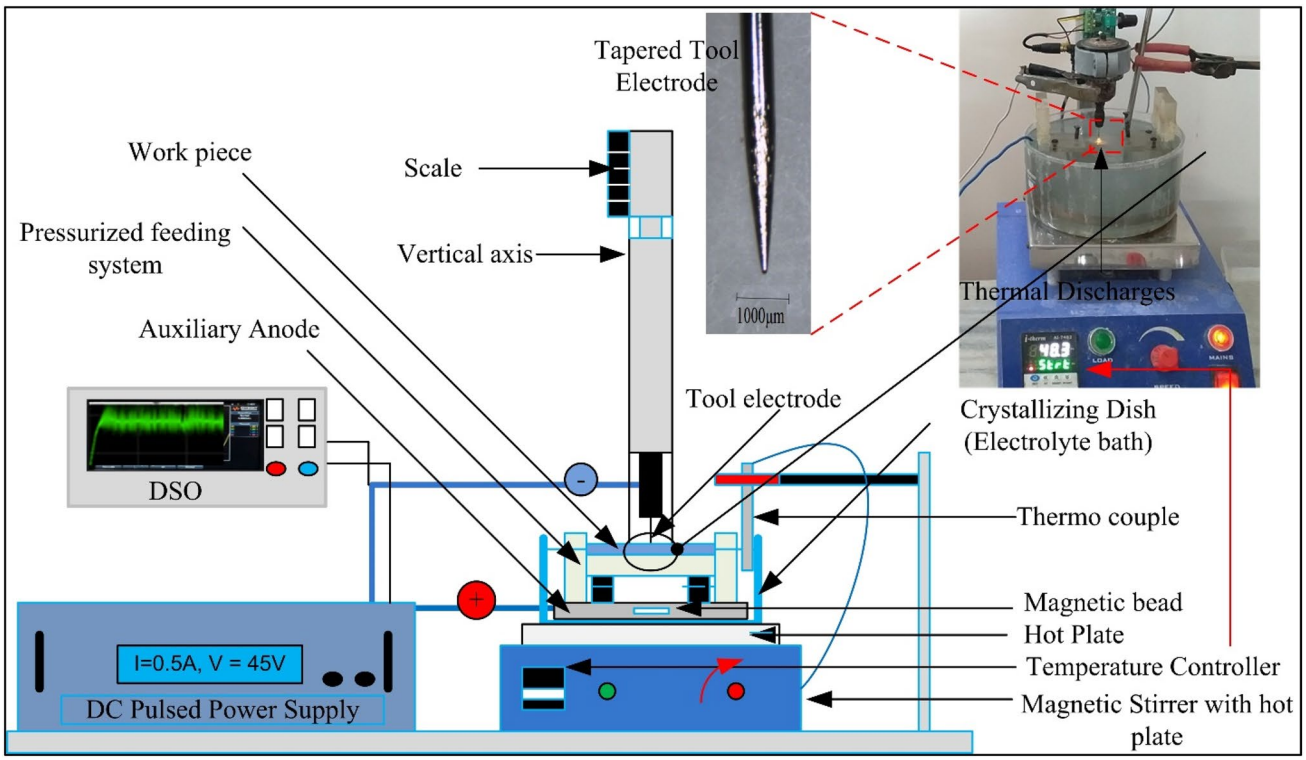

Fig. 3 Schematic diagram of T-ECDM setup

Based upon the preliminary investigation, the following Table 1 lists the study's methodological parameters, in which variable parameter is only machining time that determines the machining depth and transforms the regime from discharge to hydrodynamic that changes the energy utilization behavior of the ECDM process. The layout of the study is demonstrated in Fig. 4.

Table 1 Process parameters of ECDM

Parameters/materials	Value
Work piece material	Borosilicate glass
Electrolyte	NaOH (15% by weight)
Electrolyte temperature (TS-ECDM)	55 ℃
Electrolyte stirring (TS-ECDM)	600 rpm
Applied voltage	45 V
Tool immersion depth	2 mm
Tool electrode	Steel [pointed cylindrical (diameter = 500 um)]
Inter electrode gap (IEG)	43 mm
Auxiliary anode	SS 304 ring, diameter = 120 mm
Machining time (s)	30, 60, 90, 120, 150, 180

The layout of this experimental investigation has been demonstrated in Fig. 4. First, by keeping in view TGV application, the micro-holes were machined in borosilicate glass, followed by dimensional analysis in stereo zoom microscope (Make: Nikon, Model: SMZ745T) and dial gauge (Mitutoyo, Model: 2109S-10P) and then analysis of EUB in terms of desirable (MR and AR) and undesirable (HAZ and TWR) characteristics. Subsequently, characterization of the micro-holes was carried out in FESEM with EDS (Carl Zeiss, Gemini1, make: Germany) and profilometer (RTEC instruments) to substantiate the response outcomes.

The following subsection performs a comparative study of T-ECDM with basic-ECDM in terms of tool bubble

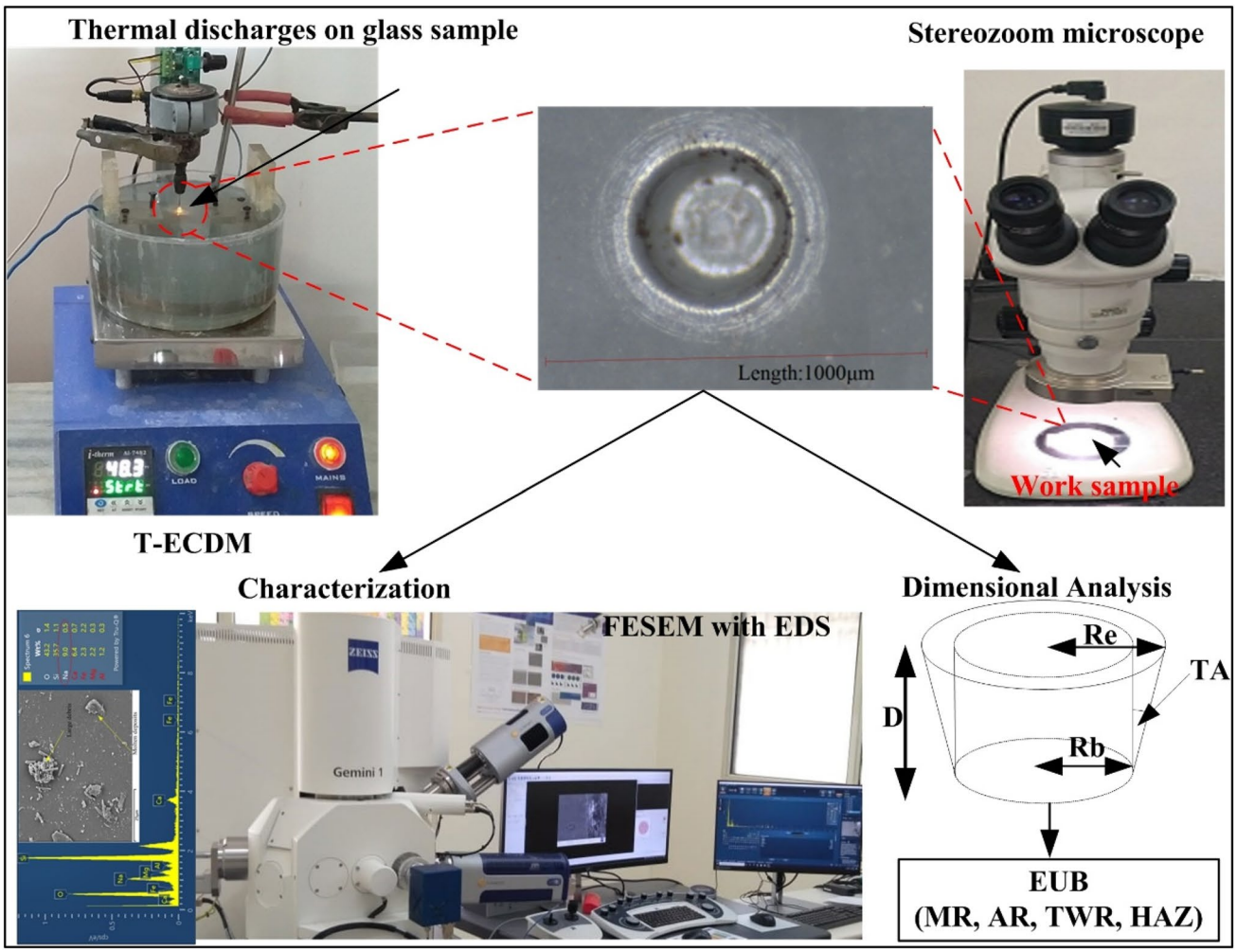

Fig. 4 Layout of the experimental investigation

interaction under various forces and its consequences on the discharge behavior and process mechanism.

2.1 Process mechanism of T-ECDM as compared to basic-ECDM

In ECDM, the application of voltage across cathode and anode forms an ECC. According to the following equations, electrochemical reactions lead to the production of H_2 and O_2 bubbles [38]:

$$\text{At Cathode}: 4H_2O + 4e^- \rightarrow 2H_2 + 4(OH)^- \quad (1)$$

$$\text{At Anode}: 4(OH)^- \rightarrow 2H_2O + O_2 + 4e^- \quad (2)$$

$$\text{Sum}: 2H_2O \rightarrow 2H_2 + O_2$$

The H_2 gas bubbles get into physical contact with each other and form a large gas bubble through coalescence, subsequently transforming into hydrogen gas film in the vicinity of cathode [15]. Wuthrich et al. applied statistical method to analyze the gas film thickness using percolation theory [39]. The gas film stability significantly affects the productivity as well as geometric characteristics of the machined geometry. A more stable gas film generates uniform discharges that increase the energy utilization behavior of the process. Since ECDM is a complex process, hence the following assumptions are made for the sake of simplification.

1. The bubbles are typically held in place by the electrode surface due to surface tension.
2. The effect of normal inertia force (F_{ni}) and tangential inertia Force (F_{ti}) on the gas bubble is neglected.
3. Through the coalescence of bubbles with similar properties, gas film has been formed.

Figure 5 depicts a schematic representation of the bubble created at the electrode surface. In stagnant condition, owing to density difference between gas and liquid, H_2 bubble experiences buoyancy force (F_b) and surface tension force (F_S) due to bubble properties.

The buoyancy force and surface tension in the vertical direction can be modeled by the following Equations [40].

$$F_b = \left(\rho_l - \rho_b\right) g V_b \quad (3)$$

$$V_b = \frac{\pi R^3}{3}(1 + \cos\gamma)^2(2 - \sin\gamma) \quad (4)$$

$$F_{sx} = -d\sigma \frac{\pi(\theta - \varnothing)}{\pi^2 - (\theta - \varnothing)^2}[\sin\theta + \sin\varnothing] \quad (5)$$

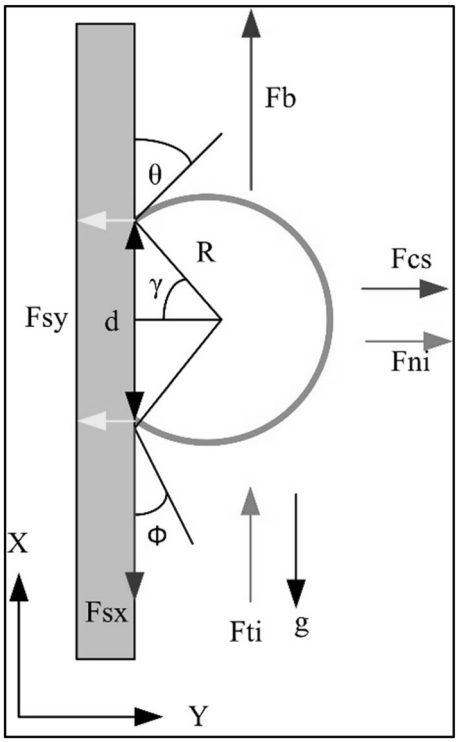

Fig. 5 Forces on H_2 gas bubble in T-ECDM

$$d = 2R \sin\gamma \quad (6)$$

where ρ_b and ρ_l represent the gas bubble density and electrolyte density, respectively. γ is the contact angle (mean) between electrode and bubble, having values for oxygen and hydrogen bubbles as 50 and 43°, respectively. R and V_b are the bubble radius and bubble volume, respectively. σ represents the surface tension at the interface of bubble with electrolyte; ($\varnothing$) and (θ) are the receding and advancing angles, respectively, owing to asymmetrical growth of the gas bubble. These angles can be expressed as follows: $\varnothing = \gamma - \Delta\gamma$ and $\theta = \gamma + \Delta\gamma$ with $\Delta\gamma < 10°$. d represents the gas bubble diameter with the electrode surface. In T-ECDM, the electrolyte temperature percolates the surface tension of the electrolyte that in turn determines the departures of the gas bubble. The surface tension of NaOH electrolyte decreases with the increase of temperature [41] and reaches zero at critical temperature. The surface tension of electrolyte with its temperature can be related as follows [42]:

$$\sigma = \frac{\varepsilon(T_c - T)}{V^{2/3}} \quad (7)$$

Here, ε is a constant having a value of $2.1 \times 10^{-7} \text{JK}^{-1}\text{mol}^{-2/3}$, V is the molar volume, and T_c is the critical temperature. From Eqs. 5, 6, and 7, the force on the gas bubble due to surface tension can be related as follows:

$$F_{sx} = -2R\ \sin\gamma\ \frac{k(T_c - T)}{V^{2/3}}\frac{\pi(\theta - \varnothing)}{\pi^2 - (\theta - \varnothing)^2}[\sin\theta + \sin\varnothing] \quad (8)$$

From the above equation, enhancement in the electrolyte temperature will result in the reduction of surface tension force. By balancing the force conditions in the vertical direction by Eqs. 9, 10 can be estimated for departure radius.

$$\sum F_x = 0 \rightarrow F_B = F_{sx} \quad (9)$$

$$R = \sqrt{\frac{6.\sin\gamma.k(T_c - T).(\theta - \varnothing).[\sin\theta + \sin\varnothing]}{(\rho_l - \rho_b).V^{2/3}.\left[\pi^2 - (\theta - \varnothing)^2\right].g.(1 + \cos\gamma)^2.(2 - \cos\gamma)}} \quad (10)$$

According to Eq. (10), the bubble departure radius will shrink as the electrolyte temperature rises. Consequently, the coalescence of tiny bubbles generates a thin stable gas film [43]. The critical voltage similarly declines owing to decrease in gas film thickness [39]. The present study has also witnessed (experimentally) the reduction in critical voltage by 1 V owing to rise in electrolyte temperature, implying the reduction of bubble departure radius according to Eq. (10). Literature reveals that a stable and uniform gas film generates uniform consistent thermal discharge [44], which enhances the energy utilization behavior of the ECDM.

As discussed earlier, electrolysis generates hydrogen bubbles and gas film in the vicinity of the tool electrode in ECDM. Whenever applied voltage surpasses the critical voltage, thermal discharges happen from gas film breakdown that starts in the areas with the strongest electric fields [40]. The electrical phenomenon including voltage/current characteristics has been to use to understand the discharge mechanism of ECDM process [45, 46]. The energy interaction through thermal discharges with the work piece results in melting and elevated temperature electrolyte etching. This paradigm changes as micro-machining progresses into deep micro-hole due to the accumulation of sludge and ineffective replenishment of electrolyte toward tool electrode tip [12]. The integration of temperature assistance and electrolyte stirring in T-ECDM can do away with these problems (electrolyte replenishment and sludge formation in the machining zone) by assisting positively in the micro-machining. The process mechanism of basic-ECDM and T-ECDM is depicted in Fig. 6a and b, respectively. The low-temperature electrolyte generates large hydrogen bubbles (according to Eq. 10) that hampers the electrolyte replenishment in the processing zone [47]. Moreover, high-viscosity electrolyte (at low temperature) causes inadequate flushing of machined products out of the machining region in ECDM (at low temperature) [48]. As a result, major thermal discharges take place at the entrance of micro-hole (Fig. 6a), resulting in the thermal damage of the workpiece [49], i.e., rise of HAZ and reduction of AR. On contrary, at elevated temperature of electrolyte in T-ECDM, the production of smaller bubbles takes place that generate a stable gas film [43]. Moreover, stray bubbles are drifted away from the entrance of micro geometry by virtue of electrolyte stirring and reduced electrolyte viscosity (at elevated temperature) enhances the penetration capability of electrolyte in the machining area that enhances the electrolyte replenishment. Furthermore, low-viscosity electrolyte also facilitates the ejection of sludge from the working zone [48]. Consequently, fresh electrolyte replenishment takes place in the machining area that facilitates the removal of sludge due to electrolyte stirring by virtue of scavenging effect [50], as shown in Fig. 6b. As a result, thermal discharges take place from the tool electrode bottom that enhances the hole depth instead of entrance diameter. Consequently, the energy utilization behavior improves in T-ECDM. The above discussion implies that in T-ECDM, the removal of material will involve melting, chemical etching at elevated temperature, and ejection of material via electrolyte stirring. To substantiate the outcomes, a comparative experimental investigation (in terms of EUB) of T-ECDM with normal ECDM has been carried out in this study.

3 Results and discussion

In this investigation, experiments are conducted to create micro-holes in the borosilicate glass for the purpose of TGV, which are required in the applications of radio frequency-based MEMS [3]. In the micro-machining of holes, the analysis was carried out to compare the EUB of basic-ECD with T-ECDM during discharge and hydrodynamic regime. In discharge regime, thermal discharges dominate the machining rate [27] and in hydrodynamic regime, etching rate dominates the machining rate. The machined micro-holes along with the state of thermal discharges are demonstrated in Fig. 7, which shows that in discharge regime, high frequency and uniform thermal discharges take place in ECDM as well as T-ECDM, resulting in the formation of uniform micro-hole with low entrance diameter. However, hydrodynamic regime exhibits non-uniform and inconsistent thermal discharges, resulting in the formation of non-uniform micro-holes with large entrance diameter.

The non-uniform thermal discharges are observed after 60 s and 90 s of machining time in basic-ECDM and T-ECDM, respectively. In T-ECDM, the elevated electrolyte temperature enhances the electrolyte conductivity [19], which accelarates the electrolysis process. As a result, the intensity of thermal discharges gets increased, which has been justified through numerical modeling. The high-intensity thermal discharges result into higher material removal [51].

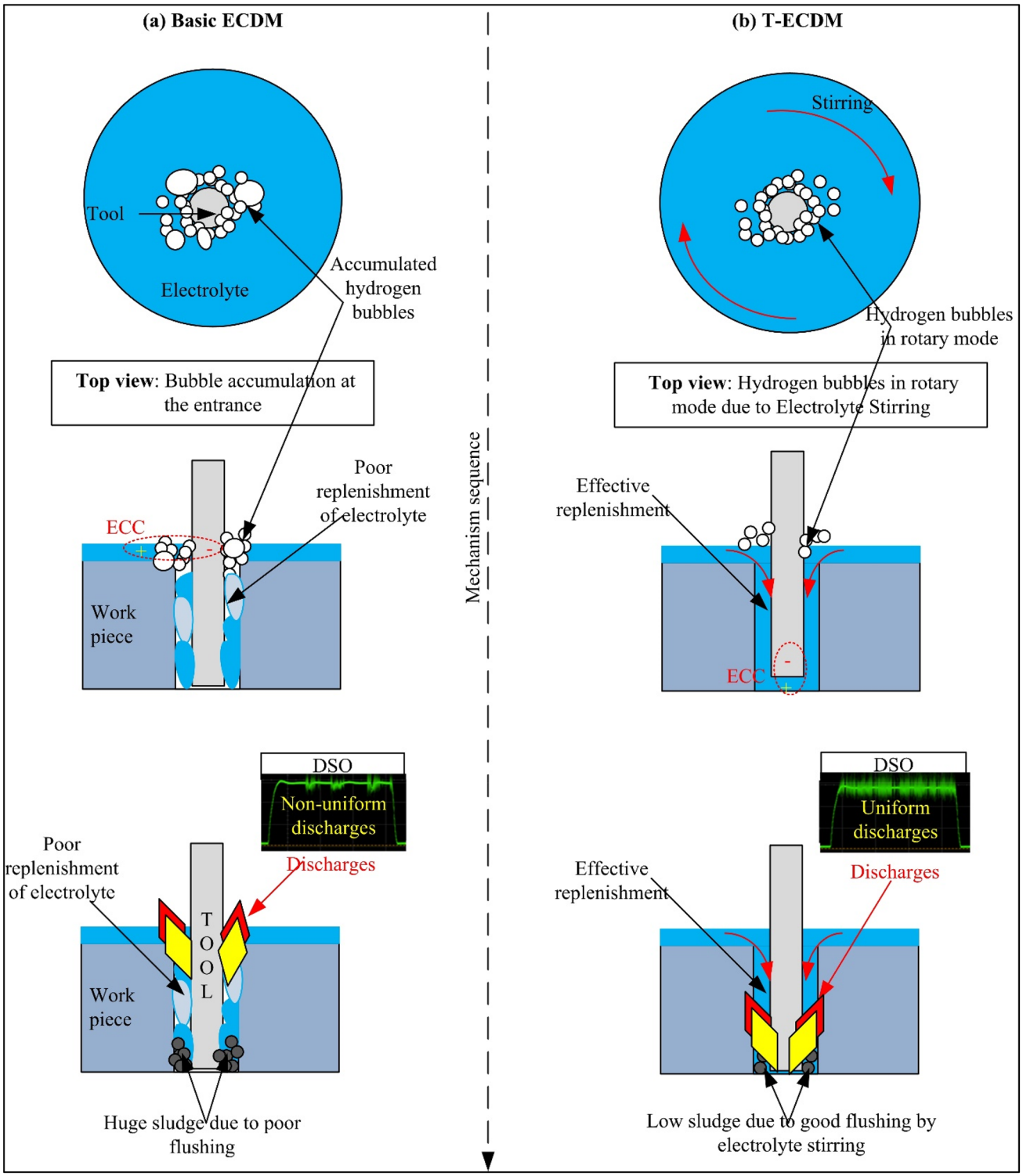

Fig. 6 Process mechanism of T-ECDM as compared to ECDM

3.1 Numerical model for the thermal analysis of machining zone

The objective of thermal analysis is to analyze the machining zone, influenced by the thermal discharges at elevated electrolyte temperature in T-ECDM process. In basic-ECDM, the electrolyte temperature was assumed equal to room temperature (30 ℃) and in T-ECDM, the electrolyte temperature was controlled at 55 ℃. Since, ECDM is a complicated micro-machining process, its mathematical

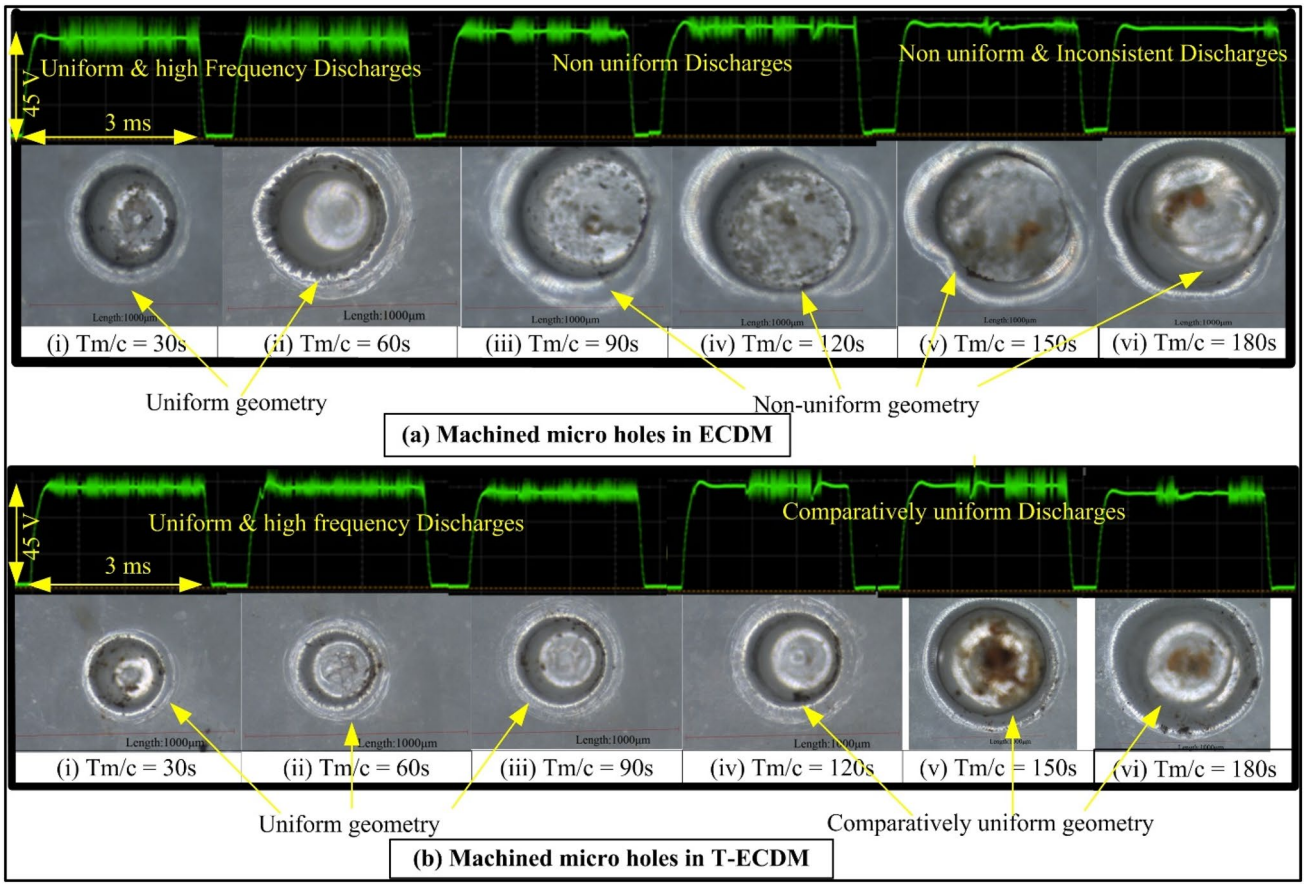

Fig. 7 Micro-holes along with discharge characteristics at different machining times (Tm/c)

modeling needs some pertinent assumptions [13]. Based on the geometry of machined surface, Literature witnessed that Gaussian distribution represents the actual shape for a growing spark as compared to uniform distribution [21]. The heat flux follows the Gaussian distribution given by Eq. (11).

$$q_r = \frac{4.45P_eVI}{\pi R_s^2} exp\left\{-4.5\left(\frac{r^2}{R_s^2}\right)\right\},\ r < R_s \tag{11}$$

where P_e is the partition energy, r indicates the radial distance, R_s is the spark radius, V represents voltage, and I (circuit current) is modeled as a function of electrical conductivity [52] and electrolyte temperature [53]. Partition energy is considered as 10%. Owing to spark energy, a 3D governing equation for transient temperature distribution (assumed to be axisymmetric) in the work piece is given by Eq. (12)

$$\frac{1}{r}\left(r\frac{\partial T}{\partial r}\right) + \frac{\partial^2 T}{\partial z^2} = \frac{\rho C_p}{K}\frac{\partial^2 T}{\partial t^2} \tag{12}$$

where ρ is the density of the workpiece and C_p and K are the specific heat (at constant pressure) and thermal conductivity, respectively. The initial and boundary conditions were considered from the literature [34]. At time $(t) = 0$, the temperature of whole domain of the workpiece is assumed to have the electrolyte temperature (T_e). As shown in Fig. 8a, the Gaussian heat flux is applied on the top surface where spark occurs and rest surface is employed with the following boundary conditions:

$$-k\left(\frac{\partial T}{\partial z}\right) = h\left(T - T_0\right) \text{ If } r > R_s \tag{13}$$

$$q_r \text{ If } r \le R_s$$

where h is the heat transfer coefficient taken as 10000 W/m^2K, the same value of heat transfer coefficient has been considered in another study also [54]. Since the temperature gradient across all other boundaries is insignificant as compared to top surface, these boundaries (Sr and Sb) are assumed to be insulated. This assumption is made on the account of a very short spark duration and given by Eq. (10).

$$\frac{\partial T}{\partial n} = 0 \text{ at } t \ge 0 \tag{14}$$

The meshed model (physics controlled, extremely fine) of borosilicate Glass is shown in Fig. 8b, for which, thermal

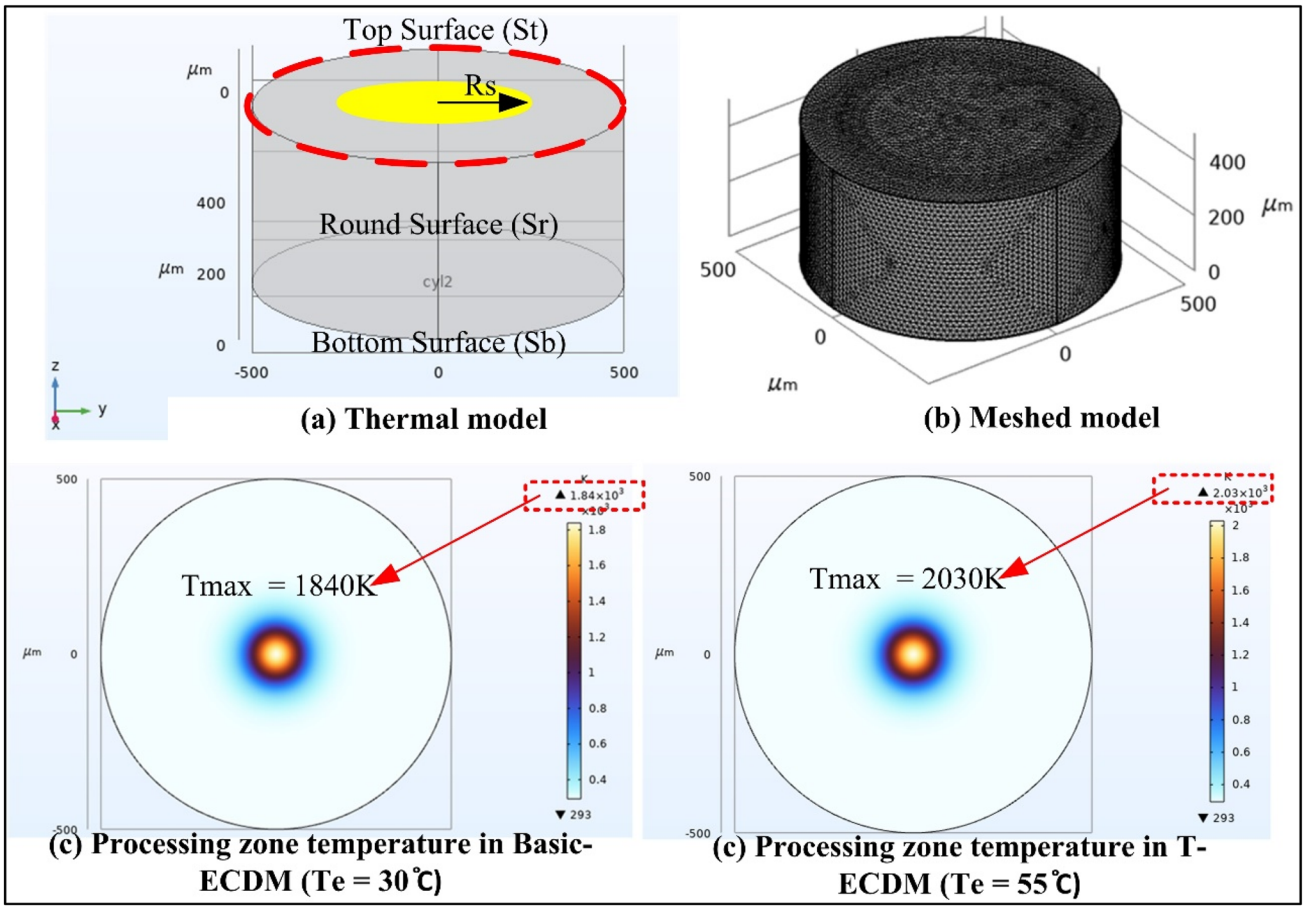

Fig. 8 Meshed model with temperature distribution in the processing zone

analysis was executed in COMSOL Multiphysics 6.0. The temperature distribution of processing zone in basic-ECDM and T-ECDM has been demonstrated in Fig. 8c and d, respectively. The highest temperature in the processing zone is 1840 K and 2030 K in basic-ECDM and T-ECDM, respectively. Consequently, material removal rate by thermal discharges (i.e., melting) remains higher in T-ECDM than basic-ECDM. Moreover, higher processing temperature elevates the electrolyte temperature, which accelerates the etching process and consequently, material removal. Therefore, material removal rate will be higher in T-ECDM than basic-ECDM. Jordan et al. [55] also reported the increase in material removal with electrolyte temperature in electro-machining.

3.2 Discharge and hydrodynamic regimes

This section deals with identifying and analyzing the discharge and hydrodynamic regimes in ECDM and T-ECDM. In ECDM, micro-machining of hole up to 300 um is considered under discharge regime and more than 300 um is considered under hydrodynamic regime [26, 27]. The hole depth with respect to machine time has been demonstrated in Fig. 9. This figure witnessed the transition from discharge to hydrodynamic regime at 47 s and 35 s in ECDM and T-ECDM, respectively, i.e., T-ECDM achieves hydrodynamic regime faster. It is also observed that at each point of machining time, hole depth remains higher in T-ECDM as compared to ECDM. As demonstrated in Figs. 7 and 8, the comparatively uniform frequent and high-intensity thermal discharges cause higher material removal in T-ECDM than basic-ECDM. At the same time, owing to higher electrolyte temperature, the material removal by chemical etching also remains higher in T-ECDM as compared to basic-ECDM, according to the following equation [56].

$$m = 3 \times 10^{7} \exp\left(-\frac{6571.3}{T}\right) \tag{15}$$

Here, m indicates the MRR (mg/hr/unit area) and T is the electrolyte temperature.

On the other hand, effective electrolyte replenishment and sludge removal leverages the energy utilization

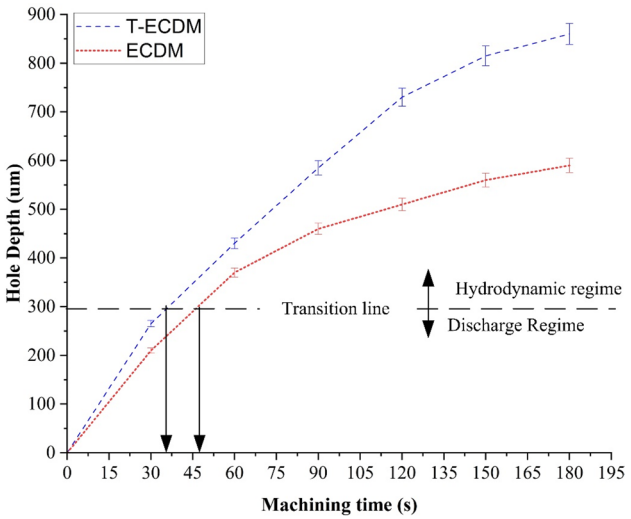

Fig. 9 Hole depth versus machining time in ECDM and T-ECDM

of T-ECDM (Fig. 6). Consequently, hole depth remains higher in discharge as well as hydrodynamic regime for T-ECDM as compared to basic-ECDM.

The following subsection discusses the comparative energy utilization of T-ECDM with basic-ECDM in terms of desirable and undesirable characteristics and then quantifies the Energy Utilization Index (EUI) according to the following equation:

$$\text{EUI} = \frac{\text{Response characteristics(T - ECDM)}}{\text{Response characteristics(basic - ECDM)}} \tag{16}$$

According to above equation, larger the better (> 1) EUI is desirable for desirable characteristics and lower the better (< 1) is desirable for undesirable characteristics.

3.3 EUB in terms of desirable characteristics

In this study, MR and AR are considered as desirable characteristics. The MR and AR symbolize the productivity and accuracy of the process. Since larger the better MR and AR are desirable, these response characteristics are classified as the desirable characteristics and defined as follows:

$$\text{MR} = \frac{\text{Hole Depth}}{\text{Machining time}}\left(\frac{um}{s}\right) \tag{17}$$

$$\text{Aspect Ratio (AR)} = \frac{\text{Hole Depth (D)}}{\text{Hole Diameter } (d)} \tag{18}$$

The cross-sections of the processed micro-holes in ECDM and T-ECDM, representing the AR, are shown in Fig. 10.

At various machining times, the corresponding values of MR and AR of micro-holes are demonstrated in Fig. 11a and b), respectively. The MR graph exhibited an exponential decrease as transition takes place from discharge to hydrodynamic regime, which is also witnessed by [56]. The AR of micro-hole exhibited an exponential increase up to a certain point and then started saturating. The statistical values pertaining to the model of MR and AR are tabulated in Table 2 (Appendix 1). From Fig. 11a and b, it can be inferred that the MR and AR remain higher in T-ECDM as compared

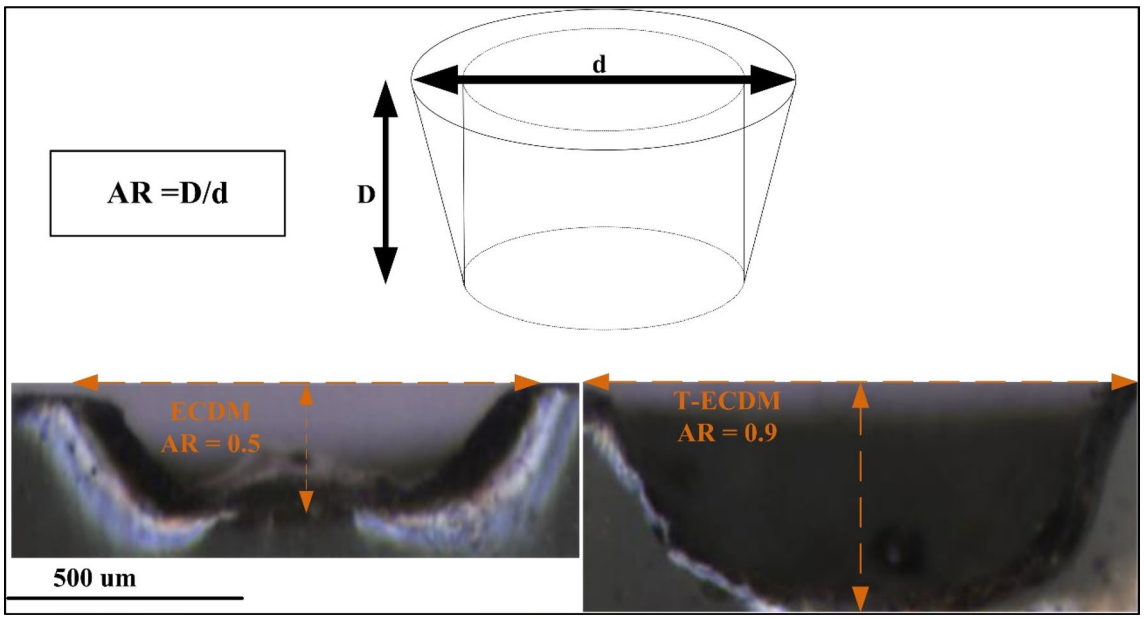

Fig. 10 Cross-sectional views representing the AR in ECDM and T-ECDM

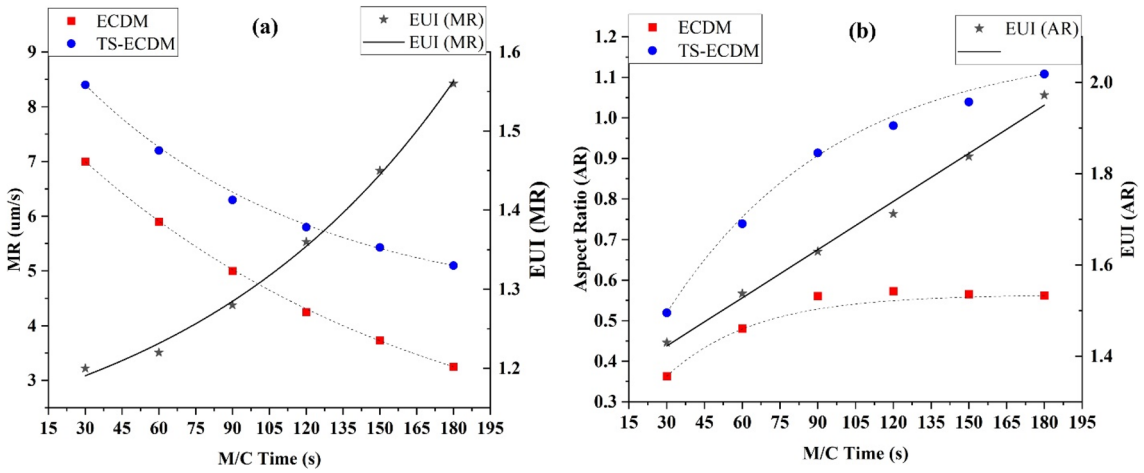

Fig. 11 Desirable characteristics (MR and AR) with respect to machining time in ECDM and T-ECDM

to ECDM. However, MR and AR exhibited a steep decline in ECDM as compared to T-ECDM. As micro-machining moves into the hydrodynamic domain, the main causes of MR reduction and AR saturation are the poor replenishment of electrolyte and accumulation of machined by-products [57]. Since, electrolyte temperature increases the electrolyte conductivity (i.e., reduction in the electrolyte resistance), the accelerated electrolysis enhances the generation rate of ions, resulting in the improvement of thermal discharges and augmented chemical etching [56]. The amount of heat produced in the machining area can be calculated by Eq. (17) [52]:

$$q = \left(V - V_w\right) \times I_m - \left[R_e \times I_m^2\right] \tag{19}$$

In Eq. (19), V represents the voltage, V_w is the water decomposition potential, R_e is the electrolyte resistance between electrodes, and I_m is the mean current. Energy generated will increase with the rise in electrolyte temperature because electrolyte resistance decreases in an inverse relationship with electrolyte temperature. Moreover, electrolyte temperature also accelerates the etching offered by the electrolyte [56]. Additionally, elevated temperature (55 ℃) and stirring action of the electrolyte improves electrolyte replenishment and flushing in the machining zone (demonstrated in Fig. 6) of T-ECDM, resulting in the improvement of energy utilization toward the hole depth instead of entrance diameter. Consequently, owing to these coupling effects, MR and AR of micro-hole remain higher in T-ECDM than ECDM in discharge as well as hydrodynamic regime.

Furthermore, EUI in terms of MR and AR remains greater than one as well as suggested an increasing function with respect to machining time. The increasing trend of EUI (during the transformation from discharge to hydrodynamic regime) for the desirable characteristics is an indication of improved EUB in T-ECDM as compared to basic-ECDM.

3.4 EUB in terms of undesirable characteristics

This section deals with the energy utilization behavior with respect to the undesirable characteristics of the process**.** Since lower the better TWR and HAZ are desirable, these response characteristics are classified as undesirable characteristics. The HAZ has been considered as the peripheral width of heat-affected zone surrounding the micro-hole and TWR has been defined by Eq. (20).

$$\text{TWR} = \frac{\text{Longitudnal tool wear}}{\text{Machining time}} \left(\frac{um}{s}\right) \tag{20}$$

In ECDM, stainless steel is the more suitable material for electrode as compared to tungsten carbide [58] and hence, stainless steel has been considered for electrode material in this study. Longitudinal tool wear represents the variation in tool length due to machining process. Figure 12 displays stereo zoom microscope pictures of TWR and HAZ. Before machining, the shape of tool tip was conical and after machining changed to flat shape due to tool wear. However, tool wear was observed almost twice in ECDM as compared to T-ECDM. The HAZ of machined micro-hole was also significantly higher in ECDM than T-ECDM.

In ECDM and T-ECDM, the behavior of tool wear with respect to machining time has been demonstrated in Fig. 13a, depicting an exponential rise in the tool wear during the transformation from discharge to hydrodynamic regime. Moreover, TWR remains highest in ECDM than T-ECDM during discharge as well as hydrodynamic regime. The statistical values of TWR models are presented in Table 3 (Appendix 1). During hydrodynamic regime in ECDM, bubble accumulation at the entrance of the machining zone and sludge formation in machining zone becomes prevalent. Additionally, the main causes of the buildup of machined

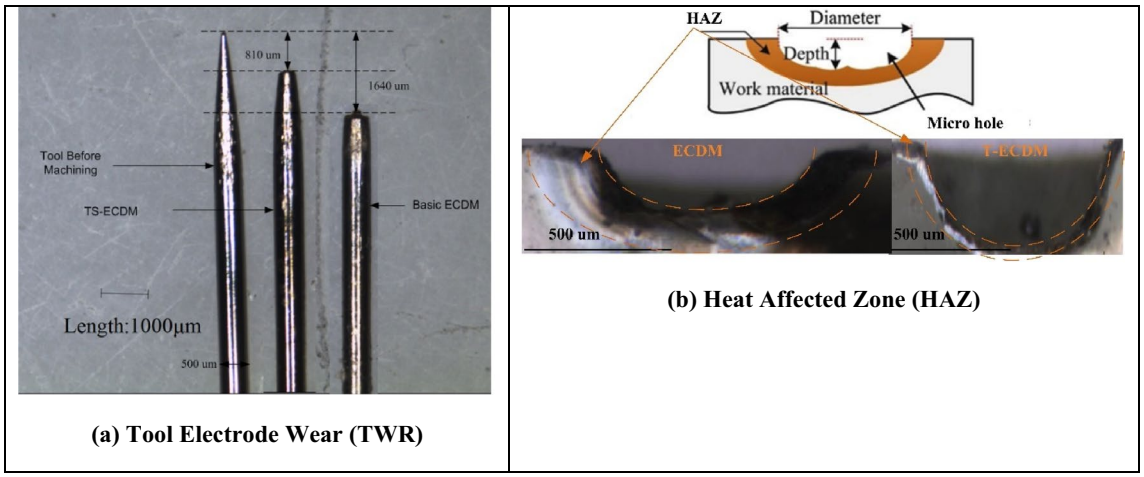

(a) Tool Electrode Wear (TWR)

(b) Heat Affected Zone (HAZ)

Fig. 12 The state of undesirable characteristics in ECDM and T-ECDM

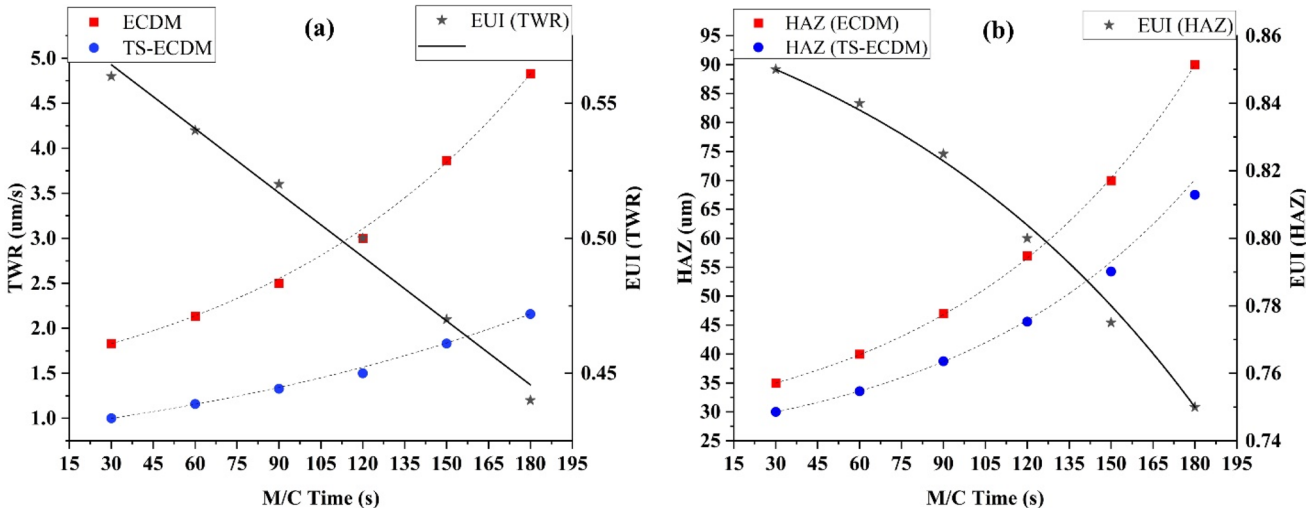

Fig. 13 Undesirable characteristics with respect to machining time in ECDM and T-ECDM

byproducts at the tip of tool electrodes are electrolyte evaporation and sludge development, decreasing the active surface area [59]. These combined effects result in poor EUB in ECDM process, i.e., more energy is utilized in the thermal degradation of tool electrode than the machining. As a result, TWR starts increasing exponentially. Although TWR also increase exponentially in T-ECDM but remains significantly lower than ECDM. The attributed reason is the improvement of process mechanism due to elevated temperature and stirring of the electrolyte (demonstrated in Fig. 6). Due to the improvement in the process mechanism of T-ECDM, more discharge energy is utilized in the enhancement of desirable characteristics [MR (Fig. 10) and AR (Fig. 11)] instead of undesirable characteristics [TWR (Fig. 13a) and HAZ (Fig. 13b)]. In basic-ECDM, electrolysis generates thick and unstable gas film, which generates non-uniform thermal discharges. Additionally, as demonstrated in Fig. 6a, owing to poor electrolyte replenishment and sludge accumulation in the machining zone of ECDM, major thermal discharges take place at the entrance of micro-hole. These combined effects increase the HAZ. Conversely, in T-ECDM, tiny bubbles generate a thin, uniform, and stable gas film that generates a uniform thermal discharges [43], which gets concentrated by virtue of electrolyte stirring. Also, due to improved electrolyte replenishment and flushing in the machining zone of T-ECDM, major thermal discharges emanate from the tool tip, having minimal influence on the heat-affected zone. These coupling effects reduce the HAZ in T-ECDM. Also, Fig. 13 infers that the EUI remains lower than the one and exhibits a declining trend for TWR as well as HAZ, implying the reduction in EUB for undesirable characteristics.

Based upon the outcomes of performance indicators, the improvement in EUI for desirable characteristics and reduction in EUI for undesirable characteristics imply the improvement of process mechanism in T-ECDM with respect to ECDM. Furthermore, the overall effect has been quantified in terms of OEUI and demonstrated using a radar graph in the subsequent section.

3.5 Overall energy utilization

In this section, OEUI is analyzed with respect to the machining time as shown in radar graph (Fig. 14). In this figure, the input parameters and output responses were normalized on 0–1 scale. The applied voltage and Energy Generated (EG) in the cell are considered as the input parameters. The energy generated is calculated by the following equation:

$$Q = V \times I \times t \tag{21}$$

where V represents voltage, t is the machining time, and I is the circuit current. The current I was modeled as a function of electrical conductivity [52] and electrolyte temperature [53]. Based on experimental conditions, the values of I were calculated as 0.27A and 0.30A in ECDM and T-ECDM, respectively. The attributed reason for higher current in T-ECDM (than ECDM) is the accelerated electrolysis (at elevated electrolyte temperature) and accordingly, EG values were also higher at various machining times (Fig. 14).

The OEUI has been considered as the output response. Based upon the energy utilization behavior of desirable and undesirable characteristics, the OEUI has been quantified as follows:

$$OEUI = \sum_{i=1}^{n1} w_i \times DC_i - \sum_{j=1}^{n2} w_j \times UC_j \tag{22}$$

In Eq. (20), $n1$ and $n2$ are the number of desirable and undesirable characteristics. Since, the present study has considered equal number of desirable (MR and AR) and undesirable characteristics (TWR and HAZ), hence $n1$ and $n2$ are considered equal to 2. The w_i and w_j are the weights assigned for desirable and undesirable characteristics based upon the importance. As the current study has considered the equal importance for desirable and undesirable characteristics, the value of w_i and w_j has been taken as one. The DC and UC represent the normalized values of desirable and characteristics, respectively. In Fig. 14, the presented values of OEUI remain significantly higher for T-ECDM than ECDM in discharge as well as hydrodynamic regime, implying the improvement in EUB.

3.6 EUB in terms of surface characteristics

To observe the effects of process mechanism of ECDM and T-ECDM on flushing and chemical etching, this section deals with the morphological and compositional analyses of the

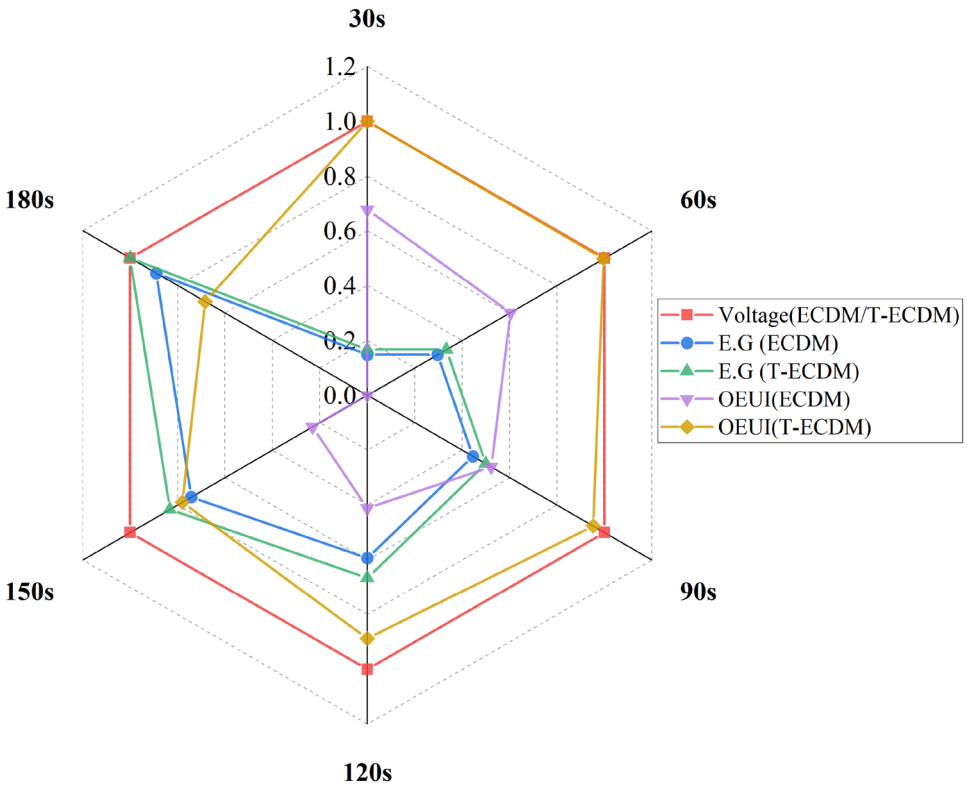

Fig. 14 Figure showing the overall energy utilization behavior with respect to machining time

processed micro-holes using a FESEM with EDS. Subsequently, the surface roughness of micro-hole was observed using profilometer. The characteristics of micro-hole processed in ECDM and T-ECDM are presented in Figs. 15 and 16, respectively. Literature reported that chemically etched surface will have less concentration of alkali metals in comparison with original glass [18]. In case of glass etching by NaOH, hydroxyl (OH^-) and sodium (Na^+) ions diffuse in the bonds of silicon oxide glass [12], resulting in material removal by electrolyte etching according to Eq. (23) [60].

$$2NaOH + SiO_2 \rightarrow Na_2SiO_3 + H_2O \quad (23)$$

The morphology and chemical composition of machined micro-holes in ECDM and T-ECDM are shown in Figs. 15a and 16a, respectively. These figures inferred that as compared to normal ECDM, T-ECDM produces the machined micro-hole with 13.33% and 48.45% reduction in sodium and silicon concentration, which implies higher etching rate in T-ECDM than ECDM. The attributed reason is the elevated electrolyte temperature (according to Eq. 15) that promotes chemical etching. From morphology of micro-holes, it can be observed that owing to higher rate of chemical etching and improved flushing in the machining zone, minor debris and insignificant molten deposits are observed in the machined micro-hole by T-ECDM as compared to ECDM. In ECDM, stagnant electrolyte causes the significant deposition of craters, while stirred electrolyte in T-ECDM reduces this deposition [36]. These combined effects of morphological and compositional outcomes from micro-holes substantiate the improved chemical etching and flushing in T-ECDM as compared to ECDM. Moreover, stirring action in electrolyte produces a homogeneous etching effect that generates the smooth surface of the micro-hole. Consequently, the surface roughness of micro-hole machined in T-ECDM resulted

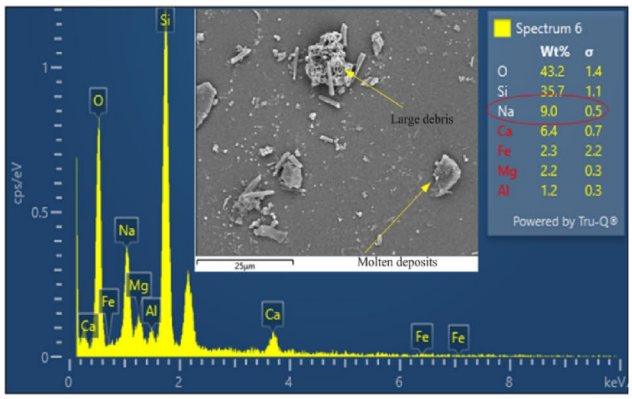

(a) Morphology and composition

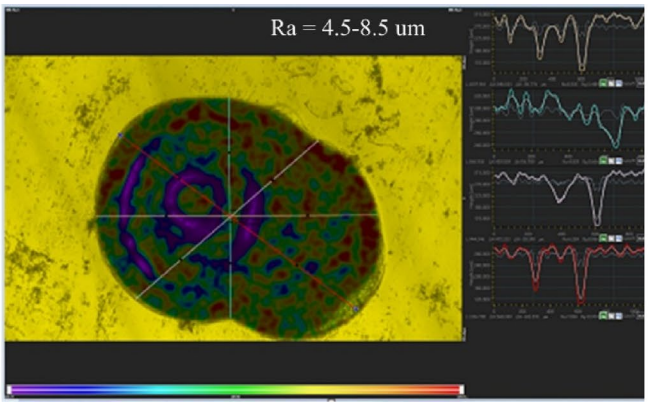

(b) Surface Roughness

Fig. 15 Characterization of micro-hole machined in ECDM

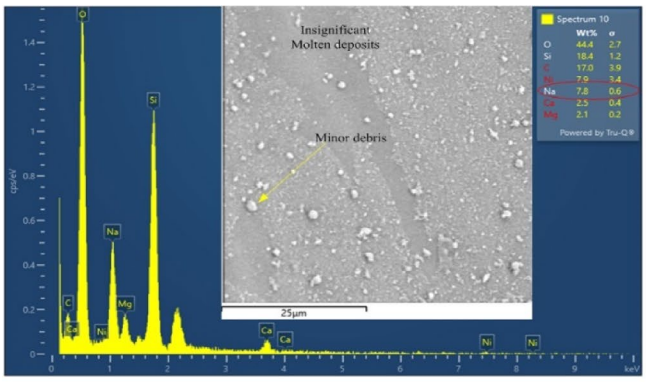

(a) Morphology and composition

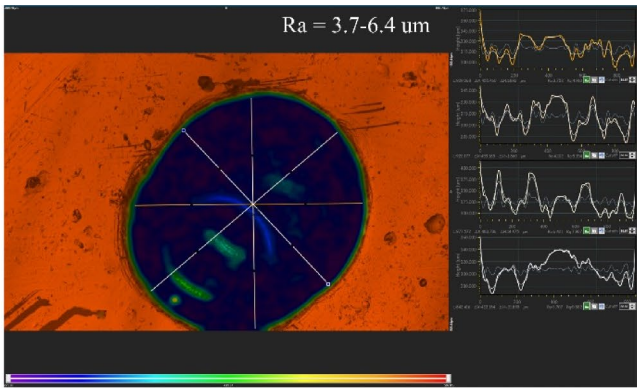

(b) Surface Roughness

Fig. 16 Characterization of micro-hole machined in T-ECDM

in lower value than ECDM, observed through profilometer (Figs. 15b and 16b). Eventually, it can be concluded that the EUB remained better in T-ECDM than ECDM in terms of surface characteristics also.

4 Conclusion

This study has successfully introduced a novel approach in ECDM using a magnetic stirrer to control the electrolyte temperature and to stir the electrolyte, which is termed T-ECDM. The controlled electrolyte temperature at a high level raises the conductivity and lowers the viscosity of the electrolyte. In T-ECDM, increased conductivity of electrolyte accelerated the electrolysis process and reduction in viscosity enhances the electrolyte replenishment in the machining area. Availability of electrolyte in the machining area coupled with stirring action resulted in better scavenging of sludge from the machining area, resulting in the improvement of EUB in the ECDM process. Comparative experimental investigation on characteristics witnessed the improvement of EUB in T-ECDM than basic-ECDM in following ways:

1. For desirable characteristics (i.e., MR and AR), EUI was found greater than one and followed an increasing function with respect to machining time.
2. For undesirable characteristics (i.e., TWR and HAZ), EUI was found less than one and followed a decreasing function with respect to machining time.
3. The OEUI was observed significantly higher during discharge as well as hydrodynamic regime.
4. The morphological and compositional analyses of the machined micro-hole had witnessed the improvement in flushing and chemical etching, which resulted in better surface finish of the micro-hole.

Based upon the outcome of this study, it can be conjectured that T-ECDM resulted in better EUB as compared to basic-ECDM. Furthermore, a controlled electrolyte temperature and homogeneous electrolyte concentration in the electrolyte bath (due to stirring action) develops stable machining conditions. Therefore, T-ECDM can be envisioned as a viable option for the micro-machining of TGV for radio frequency MEMS, lab on-chip devices, etc.

Appendix 1

The statistical values for desirable and undesirable characteristics are tabulated in Tables 2 and 3, respectively

Table 2 Statistics of models for desirable characteristics

Characteristics	MR		Characteristics	AR	
Equation	$y = A1 \times \exp(-x/t1) + y0$		Equation	$y = A1 \times \exp(x/t1) + y0$	
Plot	ECDM	TS-ECDM	Plot	ECDM	TS-ECDM
$y0$	1.189 ± 0.3035	4.279 ± 0.321	$y0$	0.56463 ± 0.0197	1.18112 ± 0.04788
$A1$	7.149 ± 0.237	5.690 ± 0.2067	$A1$	− 0.475 ± 0.15244	− 1.02833 ± 0.05605
$t1$	144.704 ± 12.134	92.952 ± 14.543	$t1$	− 34.867 ± 13.1922	− 68.00171 ± 11.989
Red. Chi-Sqr	0.00147	0.00865	Red. Chi-Sqr	5.54347E − 4	5.64765E − 4
R^2 (COD)	0.999	0.996	R^2 (COD)	0.95166	0.9929
Adj. R^2	0.999	0.994	Adj. R^2	0.91943	0.98817

Table 3 Statistics of models for undesirable characteristics

Characteristics	TWR		Characteristics	HAZ	
Equation	$y = A1 \times \exp(x/t1) + y0$		Equation	$y = A1 \times \exp(x/t1) + y0$	
Plot	ECDM	TS-ECDM	Plot	HAZ (ECDM)	(TS-ECDM)
$y0$	0.90395 ± 0.2985	0.21179 ± 0.4173	$y0$	23.18945 ± 1.108	21.18192 ± 1
$A1$	0.6937 ± 0.21839	0.65773 ± 0.36597	$A1$	8.35132 ± 0.71	6.25716 ± 1.0
$t1$	103.84511 ± 14.87	165.76444 ± 53.94	$t1$	86.5617 ± 3.00	87.44392 ± 6
Red Chi-Sqr	0.00497	0.00164	Reduced Chi-Sqr	0.1327	0.28989

Acknowledgements Not applicable.

Author contributions All authors contributed to the study conception and design. Literature survey, data analysis, and writing of the draft were performed by DB. Supervision and editing of the manuscript were carried out by AD and PK. All authors read and approved the manuscript.

Funding The authors declare that no funds, grants, or other support were received during the preparation of this manuscript.

Data availability The datasets generated during the current study are available from the corresponding author on reasonable request.

Declarations

Conflict of interest The authors have no financial or non-financial interests to disclose.

Ethical approval Not applicable.

Consent to participation Not applicable.

Consent for publication Not applicable.

References

1. Salah K (2016) TGV versus TSV: A comparative analysis. In: 2016 3rd International Conference on Advances in Computational Tools for Engineering Applications (ACTEA). IEEE, pp 49–53
2. Singh T, Mishra DK, Dixit P (2022) Effect of pulse frequency and duty cycle on electrochemical dissolution behavior of multi-tip array tool electrode for reusability in the ECDM process. J Appl Electrochem 52:667–682. https://doi.org/10.1007/s10800-021-01662-x
3. Kumar S, Dileep P, Mishra K et al (2020) Numerical and experimental analysis of high—aspect—ratio micro—tool electrode fabrication using controlled electrochemical machining. J Appl Electrochem 50:169–184. https://doi.org/10.1007/s10800-019-01380-5
4. Cheema MS, Dvivedi A, Sharma AK (2015) Tool wear studies in fabrication of microchannels in ultrasonic micromachining. Ultrasonics 57:57–64. https://doi.org/10.1016/j.ultras.2014.10.018
5. Huang SF, Liu Y, Li J et al (2014) Electrochemical discharge machining micro-hole in stainless steel with tool electrode high-speed rotating. Mater Manuf Process 29:634–637. https://doi.org/10.1080/10426914.2014.901523
6. Jha NK, Singh T, Dvivedi A, Rajesha S (2019) Experimental investigations into triplex hybrid process of GA-RDECDM during subtractive processing of MMC's. Mater Manuf Process 34:243–255. https://doi.org/10.1080/10426914.2018.1512126
7. Singh YP, Jain VK, Kumar P, Agrawal DC (1996) Machining piezoelectric (PZT) ceramics using an electrochemical spark machining (ECSM) process. J Mater Process Technol 58:24–31. https://doi.org/10.1016/0924-0136(95)02102-7
8. Malik A, Manna A (2016) An experimental investigation on developed WECSM during micro slicing of e-glass fiber epoxy composite. Int J Adv Manuf Technol 85:2097–2106. https://doi.org/10.1007/s00170-016-8858-z
9. Singh M, Singh S, Kumar S (2020) Experimental investigation for generation of micro-holes on silicon wafer using electrochemical discharge machining process. SILICON 12:1683–1689. https://doi.org/10.1007/s12633-019-00273-8
10. Doloi B, Bhattacharyya B, Sorkhel SK (1999) Electrochemical discharge machining of non-conducting ceramics. Def Sci J 49:331–338. https://doi.org/10.14429/dsj.49.3846
11. Behroozfar A, Razfar MR (2016) Experimental study of the tool wear during the electrochemical discharge machining. Mater Manuf Process 31:574–580. https://doi.org/10.1080/10426914.2015.1004685
12. Singh T, Dvivedi A, Shanu A, Dixit P (2021) Experimental investigations of energy channelization behavior in ultrasonic assisted electrochemical discharge machining. J Mater Process Technol 293:117084. https://doi.org/10.1016/j.jmatprotec.2021.117084
13. Arab J, Mishra DK, Kannojia HK et al (2019) Fabrication of multiple through-holes in non-conductive materials by electrochemical discharge machining for RF MEMS packaging. J Mater Process Technol 271:542–553. https://doi.org/10.1016/j.jmatprotec.2019.04.032
14. Gupta PK, Dvivedi A, Kumar P (2015) Developments on electrochemical discharge machining: a review of experimental investigations on tool electrode process parameters. Proc Inst Mech Eng Part B J Eng Manuf 229:910–920. https://doi.org/10.1177/0954405414534834
15. Bhattacharyya B, Doloi BN, Sorkhel SK (1999) Experimental investigations into electrochemical discharge machining (ECDM) of non-conductive ceramic materials. J Mater Process Technol 95:145–154. https://doi.org/10.1016/S0924-0136(99)00318-0
16. Wüthrich R, Fascio V (2005) Machining of non-conducting materials using electrochemical discharge phenomenon—an overview. Int J Mach Tools Manuf 45:1095–1108. https://doi.org/10.1016/j.ijmachtools.2004.11.011
17. Allagui A, Wüthrich R (2009) Gas film formation time and gas film life time during electrochemical discharge phenomenon. Electrochim Acta 54:5336–5343. https://doi.org/10.1016/j.electacta.2009.02.107
18. Kolhekar KR, Sundaram M (2018) Study of gas film characterization and its effect in electrochemical discharge machining. Precis Eng 53:203–211. https://doi.org/10.1016/j.precisioneng.2018.04.002
19. Le Bideau D, Mandin P, Benbouzid M et al (2019) Review of necessary thermophysical properties and their sensivities with temperature and electrolyte mass fractions for alkaline water electrolysis multiphysics modelling. Int J Hydrogen Energy 44:4553–4569. https://doi.org/10.1016/j.ijhydene.2018.12.222
20. Singh T, Dvivedi A (2016) Developments in electrochemical discharge machining: a review on electrochemical discharge machining, process variants and their hybrid methods. Int J Mach Tools Manuf 105:1–13. https://doi.org/10.1016/j.ijmachtools.2016.03.004
21. Kulkarni A, Sharan R, Lal GK (2002) An experimental study of discharge mechanism in electrochemical discharge machining. Int J Mach Tools Manuf 42:1121–1127. https://doi.org/10.1016/S0890-6955(02)00058-5
22. Fascio V, Langen HH, Bleuler H, Comninellis C (2003) Investigations of the spark assisted chemical engraving. Electrochem commun 5:203–207. https://doi.org/10.1016/S1388-2481(03)00018-3
23. Antil P (2020) Modelling and multi-objective optimization during ECDM of silicon carbide reinforced epoxy composites. SILICON 12:275–288. https://doi.org/10.1007/s12633-019-00122-8
24. Paul L, Hiremath SS (2022) Model prediction and experimental study of material removal rate in micro ECDM process on borosilicate glass. SILICON 14:1497–1510. https://doi.org/10.1007/s12633-021-00948-1
25. Naik R, Sathisha N (2022) Desirability function and GA-PSO based optimization of electrochemical discharge

micro-machining performances during micro-channeling on silicon-wafer using mixed electrolyte. SILICON 14:10007–10021. https://doi.org/10.1007/s12633-022-01697-5
26. Wüthrich R, Spaelter U, Bleuler H (2006) The current signal in spark-assisted chemical engraving (SACE): what does it tell us? J Micromech Microeng 16:779–785. https://doi.org/10.1088/0960-1317/16/4/014
27. Singh T, Dvivedi A (2020) On prolongation of discharge regime during ECDM by titrated flow of electrolyte. Int J Adv Manuf Technol 107:1819–1834. https://doi.org/10.1007/s00170-020-05126-y
28. Singh T, Arya RK, Dvivedi A (2020) Experimental investigations into rotary mode electrochemical discharge drilling (RM-ECDD) of metal matrix composites. Mach Sci Technol 24:195–226. https://doi.org/10.1080/10910344.2019.1636270
29. Elhami S, Razfar MR (2017) Analytical and experimental study on the integration of ultrasonically vibrated tool into the micro electro-chemical discharge drilling. Precis Eng 47:424–433. https://doi.org/10.1016/j.precisioneng.2016.09.015
30. Singh T, Appalanaidu B, Dvivedi A (2022) Improvement in energy channelization behaviour during micro hole formation in Y-SZ ceramic with magnetic field assisted ECSM process. Measurement 194:111079. https://doi.org/10.1016/j.measurement.2022.111079
31. Rathore RS, Dvivedi A (2020) Sonication of tool electrode for utilizing high discharge energy during ECDM. Mater Manuf Process 35:415–429. https://doi.org/10.1080/10426914.2020.1718699
32. Gupta PK (2018) Effect of electrolyte level during electro chemical discharge machining of glass. J Electrochem Soc 165:E279–E281. https://doi.org/10.1149/2.1021807jes
33. Rahman MA, Saghir MZ (2014) Thermodiffusion or Soret effect: historical review. Int J Heat Mass Transf 73:693–705. https://doi.org/10.1016/j.ijheatmasstransfer.2014.02.057
34. Goud M, Sharma AK (2017) A three-dimensional finite element simulation approach to analyze material removal in electrochemical discharge machining. Proc Inst Mech Eng Part C J Mech Eng Sci 231:2417–2428. https://doi.org/10.1177/0954406216636167
35. Paul L, George D (2018) ScienceDirect effects of preheating electrolyte in micro ECDM process. Mater Today Proc 5:11882–11887. https://doi.org/10.1016/j.matpr.2018.02.161
36. Jawalkar CS, Sharma AK, Kumar P (2020) Innovations in electro chemical discharge machining process through electrolyte stirring and tool rotations. Int J Mach Mach Mater 22:487–503. https://doi.org/10.1504/IJMMM.2020.111354
37. Kumar S, Dvivedi A (2019) On effect of tool rotation on performance of rotary tool micro-ultrasonic machining. Mater Manuf Process 34:475–486. https://doi.org/10.1080/10426914.2018.1512130
38. Weier T, Landgraf S (2013) The two-phase flow at gas-evolving electrodes: bubble-driven and Lorentz-force-driven convection. Eur Phys J Spec Top 220:313–322. https://doi.org/10.1140/epjst/e2013-01816-1
39. Wüthrich R, Hof LA (2006) The gas film in spark assisted chemical engraving (SACE)—A key element for micro-machining applications. Int J Mach Tools Manuf 46:828–835. https://doi.org/10.1016/j.ijmachtools.2005.07.029
40. Zhang D, Zeng K (2012) Evaluating the behavior of electrolytic gas bubbles and their effect on the cell voltage in alkaline water electrolysis. Ind Eng Chem Res 51:13825–13832. https://doi.org/10.1021/ie301029e
41. Dudita M, Daguenet-Frick X, Gantenbein P (2016) Seasonal Thermal Energy Storage with Aqueous Sodium Hydroxide—Experimental Methods for Increasing the Heat and Mass Transfer by Improving Surface Wetting. In: Proceedings of EuroSun2016. International Solar Energy Society, Freiburg, pp 1–9
42. Glasser L (2021) Volume-based thermodynamics of ionic liquids and molten salts: surface tension and the Eötvös equation. J Chem Thermodyn 161:106520. https://doi.org/10.1016/j.jct.2021.106520
43. Cheng CP, Wu KL, Mai CC et al (2010) Study of gas film quality in electrochemical discharge machining. Int J Mach Tools Manuf 50:689–697. https://doi.org/10.1016/j.ijmachtools.2010.04.012
44. Singh T, Dvivedi A (2022) Impact of gas film thickness on the performance of RM-ECDM process during machining of glass. Mater Manuf Process 37:652–663. https://doi.org/10.1080/10426914.2021.1945092
45. Singh T, Rathore RS, Dvivedi A (2020) Experimental investigations, empirical modeling and multi objective optimization of performance characteristics for ECDD with pressurized feeding method. Measurement 149:107017. https://doi.org/10.1016/j.measurement.2019.107017
46. Crichton IM, McGeough JA (1985) Studies of the discharge mechanisms in electrochemical arc machining. J Appl Electrochem 15:113–119. https://doi.org/10.1007/BF00617748
47. Maillard P, Despont B, Bleuler H, Wüthrich R (2007) Geometrical characterization of micro-holes drilled in glass by gravity-feed with spark assisted chemical engraving (SACE). J Micromech Microeng 17:1343–1349. https://doi.org/10.1088/0960-1317/17/7/017
48. Abou Ziki JD, Fatanat Didar T, Wüthrich R (2012) Micro-texturing channel surfaces on glass with spark assisted chemical engraving. Int J Mach Tools Manuf 57:66–72. https://doi.org/10.1016/j.ijmachtools.2012.01.012
49. Appalanaidu B, Dvivedi A (2022) On the use of sacrificial layer in ECDM process for form accuracy. J Manuf Process 79:219–232. https://doi.org/10.1016/j.jmapro.2022.04.043
50. Jain VK, Chak SK (2000) Electrochemical spark trepanning of alumina and quartz. Mach Sci Technol 4:277–290. https://doi.org/10.1080/10940340008945710
51. Sharma S, Singh T, Dvivedi A (2022) A review on developments in electrolytes and their feeding methods for ECDM process. SILICON. https://doi.org/10.1007/s12633-022-02134-3
52. Jain VK, Dixit PM, Pandey PM (1999) On the analysis of the electrochemical spark machining process. Int J Mach Tools Manuf 39:165–186. https://doi.org/10.1016/S0890-6955(98)00010-8
53. Hua Z, Jiawen X (2010) Modeling and experimental investigation of laser drilling with jet electrochemical machining. Chinese J Aeronaut 23:454–460. https://doi.org/10.1016/S1000-9361(09)60241-7
54. Mishra DK, Arab J, Magar Y, Dixit P (2019) High aspect ratio glass micromachining by multi-pass electrochemical discharge based micromilling technique. ECS J Solid State Sci Technol 8:P322–P331. https://doi.org/10.1149/2.0191906jss
55. Jordan P (2016) Experimental Studies in Electro-Machining. Journal of Engineering for industry. Transactions of ASME, 945–953.
56. Jalali M, Maillard P, Wüthrich R (2009) Toward a better understanding of glass gravity-feed micro-hole drilling with electrochemical discharges. J Micromech Microeng. https://doi.org/10.1088/0960-1317/19/4/045001
57. Sarkar BR, Doloi B, Bhattacharyya B (2006) Parametric analysis on electrochemical discharge machining of silicon nitride ceramics. Int J Adv Manuf Technol 28:873–881. https://doi.org/10.1007/s00170-004-2448-1
58. Ziki JDA, Wüthrich R (2012) Tool wear and tool thermal expansion during micro-machining by spark assisted chemical engraving. Int J Adv Manuf Technol 61:481–486. https://doi.org/10.1007/s00170-011-3731-6
59. Sabahi N, Razfar MR (2018) Investigating the effect of mixed alkaline electrolyte (NaOH + KOH) on the improvement of machining efficiency in 2D electrochemical discharge machining

(ECDM). Int J Adv Manuf Technol 95:643–657. https://doi.org/10.1007/s00170-017-1210-4
60. Rajurkar KP, Sundaram MM, Malshe AP (2013) Review of electrochemical and electrodischarge machining. Procedia—Soc Behav Sci 6:13–26. https://doi.org/10.1016/j.procir.2013.03.002